Application of the Time-Independent Wave Packet Reactant−Product Decoupling Method to the ($J = 0$) Li + HF Reaction

Stuart C. Althorpe* and Donald J. Kouri

Department of Chemistry and Department of Physics, University of Houston, Houston, Texas 77204-5641

David K. Hoffman

Department of Chemistry and Ames Laboratory, Iowa State University, Ames, Iowa 50011

Received: April 24, 1998; In Final Form: July 20, 1998

The time-independent wave packet reactant−product decoupling (TIW−RPD) method is a new method for calculating state-to-state reaction probabilities, which we recently developed by extending the original reactant−product decoupling method of Peng and Zhang (Peng, T.; Zharg, J. Z. H. *J. Chem. Phys.* **1996**, *105*, 6072; Zhu, W.; Peng, T.; Zhang, J. Z. H. *J. Chem. Phys.* **1997**, *106*, 1742). In the TIW−RPD method, the nuclear dynamics Schroedinger equation is partitioned into a set of completely decoupled equations, each of which describes the nuclear dynamics in either the reactant channel, one of the product channels, or the strong-interaction region. In this paper we apply the TIW−RPD method to the (three-dimensional) Li + HF → LiF + H ($J = 0$) reaction. We also describe an improvement to the reactant channel part of the method. The state-to-state reaction probabilities for Li + HF converge very well with respect to the size of the strong-interaction region, demonstrating that the TIW−RPD method is robust enough to be applied to a wide range of chemical reactions, including those in which the dynamics are influenced by a long-range potential energy surface.

1. Introduction

The time-independent wave packet reactant−product decoupling (TIW−RPD) method[1] is a new method for solving the nuclear dynamics Schroedinger equation for state-to-state reactive scattering. The method is the first application to state-to-state reactive scattering of a result obtained several years ago by Seideman and Miller,[2] who showed that, when calculating the *cumulative* reaction probabilities, it is possible to calculate the wave function in the strong-interaction region (in which the exchange of atoms occurs) without calculating the wave function in any of the reactant and product channels (in which energy is redistributed among the reactants or products but in which no exchange of atoms occurs). In the TIW−RPD method, the wave function is calculated separately in the strong-interaction region and in each of the reactant and product channels.

The method of Seideman and Miller made use of a method that had previously been developed by Neuhauser et al.[3] for calculating the total (initial state selected) reaction probabilities. In any chemical reaction there exists a "point-of-no-return" at the start of each product channel, beyond which, to a given degree of accuracy, the flux of the wave function is entirely outgoing. Neuhauser et al. showed that, by placing absorbing potentials after the points-of-no-return, it is possible to calculate the wave function in the *reactant-interaction region* (the region of coordinate space enclosing the reactant channel and the strong interaction region) and thereby to obtain the total reaction probabilities. In the method of Seideman and Miller,[2] an additional absorbing potential is placed at the start of the reactant channel beyond the point-of-no-return, so that the strong-interaction wave function is now enclosed in a box consisting of the absorbing potentials and the repulsive walls of the (interaction) potential. The size of the box is a convergence parameter, which may be increased until the cumulative reaction probabilities have converged to the desired accuracy.

Very recently, Peng and Zhang[4] have developed a way of extending the method of Neuhauser et al., so that, after calculation of the wave function in the reactant-interaction region, it is possible to re-emit the absorbed parts of the wave function and propagate them down the product channel. This yields the wave function in the product channel, and hence the state-to-state reaction probabilities. Peng and Zhang call their method the reactant−product decoupling (RPD) method, because the calculation in the product channel is completely decoupled from the calculation in the reactant-interaction region.

The TIW−RPD method[1] is an extended version of Peng and Zhang's RPD method, whereby the calculation in the reactant-interaction region is further decoupled[5] into a calculation in the reactant channel and a calculation in the strong-interaction region. In the latter, the wave function is enclosed in a box, exactly as in the method of Seideman and Miller.[2] The calculations are performed within the time-independent wave packet (TIW) formalism,[6,7] which permits the use of an efficient wave packet propagator[8,9] based on the Chebyshev propagator.[10] Full details of the TIW−RPD method and of the propagator may be found in refs 1 and 8. A summary of the method is also given in this paper (section 2A), along with a description of a new development to the reactant channel part of the method (section 2B).

The main purpose of this paper is to report an application of the TIW−RPD method to the ($J = 0$) Li + HF → LiF + H reaction (Section 3). Unlike the H + H_2 reaction (on which

* Corresponding author. Present address: Steacie Institute, National Research Council, Ottawa, Ontario K1N OR6, Canada.

10.1021/jp981992m CCC: $15.00
Published on Web 10/17/1998

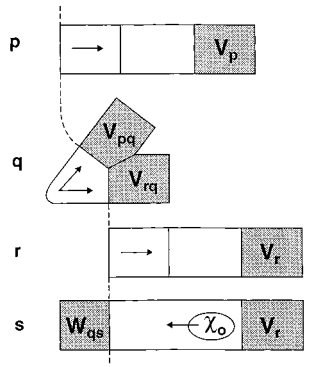

Figure 1. Schematic illustration of how the TIW−RPD method decouples the reaction dynamics in the strong-interaction region (*q*) from the dynamics in the reactant channel (*r* and *s*) and the product channel (*p*). The shaded areas represent the partitioning potentials W_{qs}, V_{rq}, and V_{pq} (see text). The dashed line connects the reactant and product points-of-no-return.

we tested the method in ref 1), the Li + HF reaction has a long-range potential energy surface, with wells in both the reactant and the product channel, and a double barrier in the product channel. Previous calculations of the state-to-state reaction probabilities by Gögtas et al.[11] and Parker et al.[12] showed that the surface is capable of supporting long-lived Feshbach resonances, which can extend outward down both the product and the reactant channel. The Li + HF reaction is thus a particularly challenging reaction on which to test the TIW−RPD method. When presenting the results (Section 3A), we pay close attention to how the size of the box (enclosing the strong-interaction region) affects the resonance peaks observed in the state-to-state reaction probabilities. We discuss the results in Section 3.B and conclude the paper in Section 4.

2. Time-Independent Wave Packet Reactant−Product Decoupling Method

A. Summary of the Method. In the TIW−RPD method,[1] the coordinate space of a reaction with *P* product arrangements is partitioned into $P + 3$ overlapping regions, which we may label the *p*, *q*, *r*, and *s* regions. There are *P p* regions, each of which encloses one of the product channels, and one each of the *q* region, which encloses the strong-interaction region, the *r* region, which encloses the reactant channel, and the *s* region, which also encloses the reactant channel. The *s* region is used to propagate the initial wave packet down the reactant channel toward the strong-interaction region; the *r* region is used to propagate the inelastically scattered component of the wave packet back down the reactant channel. The partitioning is illustrated schematically in Figure 1, for the simplest example of a two-dimensional reaction with one product channel ($P = 1$).

The regions overlap at the shaded areas W_{qs}, V_{rq}, and V_{pq}, each of which represents a *partitioning potential*. The latter are artificial potentials that either reflect or absorb the wave packet so as to keep it within a given region; the overlap of the wave packet with a partitioning potential is stored on disk and is subsequently retrieved to act as a source term for a wave packet propagation in another region. The potentials V_{rq} and V_{pq} are (the moduli of) negative imaginary absorbing potentials, which are placed after the points-of-no-return at the start of the reactant and product channels. Together with the repulsive walls of the reactive potential energy surface, the potentials V_{rq} and V_{pq} completely enclose the strong-interaction region, as is done in the flux−flux autocorrelation method (for calculating cumulative reaction probabilities) of Seideman and Miller.[2] The other partitioning potential W_{qs} is taken, in this paper,[13] to be a real, reflecting potential that prevents the initial wave packet (χ_0 in Figure 1) from reaching the boundaries of the *s*-region. (We shall discuss the choice of W_{qs} in section 2B below.) Additional absorbing potentials V_r and V_p are placed at the ends of the reactant and product channels; these are *not* partitioning potentials—they simply prevent the wavepacket reflecting off the grid boundaries.

The wave function in each of the regions *p*, *q*, *r*, and *s* is calculated by solving a completely decoupled *time-independent wave packet*[6] (TIW) equation. Starting with the formal solution $\chi(t) = U(t)\chi(0)$ to the time-dependent Schroedinger equation, the TIW equation, obtained by taking a half-Fourier transform, is

$$\xi^+(E) = \frac{i}{2\pi} G^+(E)\chi(0) \tag{1}$$

Note that the causal Green's operator $G^+(E)$ is the half-Fourier transform of the time-evolution operator $U(t)$. It can be shown[6] that, between the initial wave packet $\chi(0)$ and the (interaction) potential, the TIW wave function $\xi^+(E)$ is proportional to the Lippmann−Schwinger solution of the time-independent Schroedinger equation.

In the TIW−RPD method,[1] eq 1 is taken to be the TIW equation corresponding to the nuclear dynamics Schroedinger equation for reactive scattering. Rather than solve this equation directly, we solve the set of *decoupled* equations[14]

$$\xi_s{}^+(E) = \frac{i}{2\pi} G_s{}^+(E)\chi_0 \tag{2}$$

$$\xi_q{}^+(E) = -G_q{}^+(E)W_{qs}\xi_s{}^+(E) \tag{3}$$

$$\xi_r{}^+(E) = -G^+(E)\Gamma_{rq}(E)\xi_q{}^+(E) \tag{4}$$

$$\xi_p{}^+(E) = -G^+(E)\Gamma_{pq}(E)\xi_q{}^+(E) \qquad \text{for each } p \tag{5}$$

Here $G_s{}^+(E)$ is the Green's function corresponding to the Hamiltonian $H + W_{qs}$, and $G_q{}^+(E)$ is the Green's function corresponding to the Hamiltonian $H + \Gamma_{rq}(E) + \sum_p \Gamma_{pq}(E)$. The $\Gamma(E)$ terms in this expression and in eqs 4 and 5 are the absorbing potentials V_{rq} and V_{pq} multiplied by functions of the total energy *E*.[15] It may be shown[1,8] that, to a given degree of accuracy (which increases as the points-of-no-return are moved outward), the solutions $\xi_\lambda{}^+(E)$, $\lambda = p, q, r, s$, add up to give

$$\xi^+(E) = \xi_s{}^+(E) + \xi_q{}^+(E) + \xi_r{}^+(E) + \sum_p \xi_p{}^+(E) \tag{6}$$

and that each solution is confined to the corresponding *p*, *q*, *r*, *s* region of Figure 1. Solving each of eqs 2−5 thus yields the component of $\xi^+(E)$ in either the reactant channel $[\xi_s{}^+(E) + \xi_r{}^+(E)]$, the *p*th product channel $[\xi_p{}^+(E)]$ or the strong-interaction region $[\xi_q{}^+(E)]$.

We have developed an efficient method[1,8] of solving eqs 2−5 that is based on the Chebyshev propagator.[10] Each component $\xi_\lambda{}^+(E)$, $\lambda = p, q, r, s$, is expanded as

$$\xi_\lambda{}^+(E) = \frac{1}{2\pi\Delta H \sin\phi} \sum_{n=0}^{N} e^{-in\phi}\eta_{\lambda n} \qquad \lambda = p, q, r, s \tag{7}$$

where $\phi = \cos^{-1}[(E - \bar{H})/\Delta H]$, and $\bar{H}$ and ΔH are scaling

parameters, chosen such that the spectrum of $H_{\text{norm}} = (H - \bar{H})/\Delta H$ is confined to $[-1, 1]$. The functions $\eta_{\lambda n}$ are propagated by a set of Chebyshev-like recursion relations, in which the action of the (normalized) Hamiltonian H_{norm} is evaluated within the appropriate *p*, *q*, *r*, or *s* region of coordinate space. The recursion relations used in this paper are given in the Appendix.

After eqs 2−5 are solved, the state-to-state reaction and inelastic probabilities are extracted from $\xi_p^+(E)$ and $\xi_r^+(E) + \xi_s^+(E)$. To a given accuracy, these probabilities can be converged to the numerically exact results (which would have been obtained by solving eq 1 directly), simply by increasing the size of the *q* region until the points-of-no-return are located far enough down the reactant and product channels. In section 3 we report the results of testing this convergence on the Li + HF reaction.

B. Basis Sets and Coordinates. When each of eqs 2−5 is solved, the action of the Hamiltonian needs to be evaluated within just one of the regions *p*, *q*, *r*, *s* and can thus be represented in terms of the coordinate system and basis set that best describe the dynamics in that region. One expects the *r* and *p* regions to require much smaller basis sets than the *q* region, since it is in the *q* region that the exchange of atoms takes place. In each of the *r* and *p* regions, the atoms remain in either the reactant or the *p*th product configuration, so that an efficient basis set can be constructed from the isolated reactants or products. In the *s* region the basis set must in general be a mixture of the *r* and the *q* basis sets, since the *s* region encloses the reactant channel plus part of the strong-interaction region (where it overlaps the *q* region at W_{qs}).

In refs 1 and 9, we developed basis sets and coordinates for solving eqs 2−5 in the general case of the ($J = 0$) A + BC → AC + B reaction. The *s*, *r*, and *q* Hamiltonians are represented in terms of reactant arrangement (A + BC) Jacobi coordinates, and the *p* Hamiltonian is represented in terms of product arrangement (AC + B) Jacobi coordinates. Each Hamiltonian takes the well-known form

$$H = -\frac{\hbar^2}{2\mu R}\frac{\partial^2}{\partial R^2}R - \frac{\hbar^2}{2mr}\frac{\partial^2}{\partial r^2}r + \left[\frac{\hbar^2}{2\mu R^2} + \frac{\hbar^2}{2mr^2}\right]\mathbf{j}^2 + V(R, r, \theta) \quad (8)$$

where *R* is the distance between A (B) and the center of mass of BC (AC); *r* is the bond length of BC (AC); θ is the angle between *R* and *r*; and μ and *m* are the appropriate reduced masses. In each region, the *R* coordinate is represented by a discrete distributed approximating functional[16−18] (DAF) representation, which consists of a grid of equally spaced discrete points along the *R* coordinate. The θ coordinate is represented by a Gauss−Legendre discrete variable representation[19] (DVR). The *r* coordinate is represented by different grid representations in different regions: In the *q* region, the *r* coordinate is represented by a discrete DAF, similar to the one used to represent *R*. In the *r* and *p* regions, the *r* coordinate is represented in terms of a DVR, obtained from the vibrational wave functions of either BC or AC.

We now depart from ref 1 and show how the DVR used to represent the *r* coordinate in the *r* region can also be used (efficiently) to represent the *r* coordinate in the *s* region. As we mentioned above, the basis set in the *s* region must, in general, describe the dynamics in the reactant channel, where the atoms remain in the A + BC configuration, plus the more complicated dynamics in the part of the strong-interaction region that overlaps W_{qs}. If W_{qs} is suitably chosen, however, the dynamics in the strong-interaction part of the *s* region can be constrained such that the atoms remain in the A + BC configuration throughout the entire *s* region. We choose a W_{qs} of the form

$$W_{qs}(R, r, \theta) = V(R_{qs}, r, \theta) - V(R, r, \theta) + V_{\text{ramp}}(R) \quad (9)$$

where R_{qs} is the reactant point-of-no-return (located to the right of W_{qs} in Figure 1), $V(R, r, \theta)$ is the potential energy surface (of the reaction), and $V_{\text{ramp}}(R)$ is a reflecting ramp. It can be seen that, with this choice of W_{qs}, the potential in the total Hamiltonian $H + W_{qs}$ is equal to $V(R, r, \theta)$ for $R > R_{qs}$ and $V(R_{qs}, r, \theta) + V_{\text{ramp}}(R)$ for $R < R_{qs}$. This potential keeps the atoms within the A + BC configuration and prevents the wave packet from hitting the edges of the *s* region grid.

We emphasize that, even with the above choice of W_{qs}, the solutions of eqs 2−5 still satisfy eq 1 (to the same degree of accuracy), because the component in $\xi_s^+(E)$ that is reflected (artificially) down the reactant channel [by $V_{\text{ramp}}(R)$] is canceled out by an equal and opposite component in $\xi_r^+(E)$.

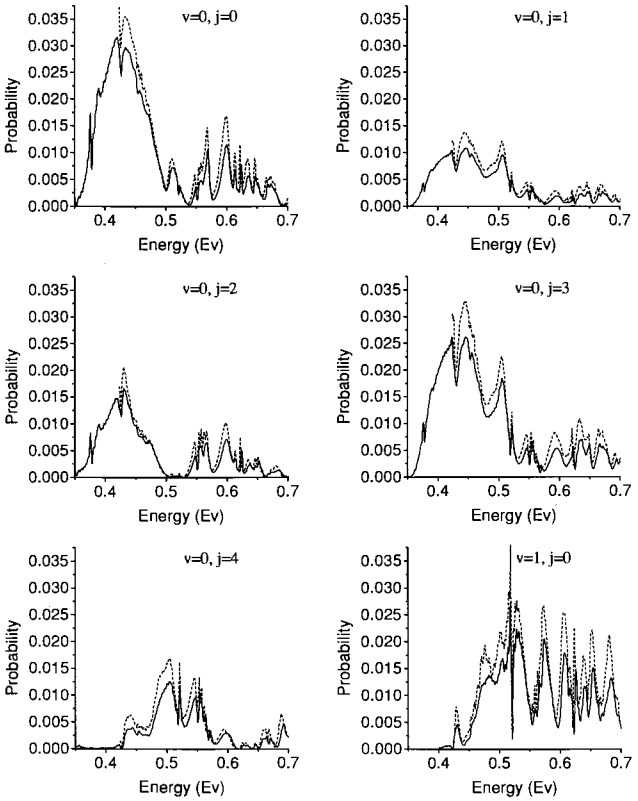

Figure 2. State-to-state reaction probabilities $R[(v_0 = 0, j_0 = 0) \rightarrow (v, j)]$ for the Li + HF(v_0, j_0) → LiF(v, j) + H reaction, calculated by the TIW−RPD method (solid line) and taken from the results of Göğtas et al.[11] (dashed line).

3. Application to the Li + HF Reaction (for $J = 0$)

A. Numerical Details. We calculated state-to-state reaction probabilities and inelastic probabilities for the ($J = 0$) Li + HF → LiF + H reaction, applying the TIW−RPD method as summarized above. Selected results are presented in Figure 2 (state-to-state reaction probabilities) and Figure 3 (state-to-state inelastic probabilities).

The numerical parameters used in the calculation are given in Table 1. Most of these parameters are either self-explanatory or have been defined in Section 2. The wave packet parameters, x_0, x_I, and k_{av}, are defined such that the initial wave packet is

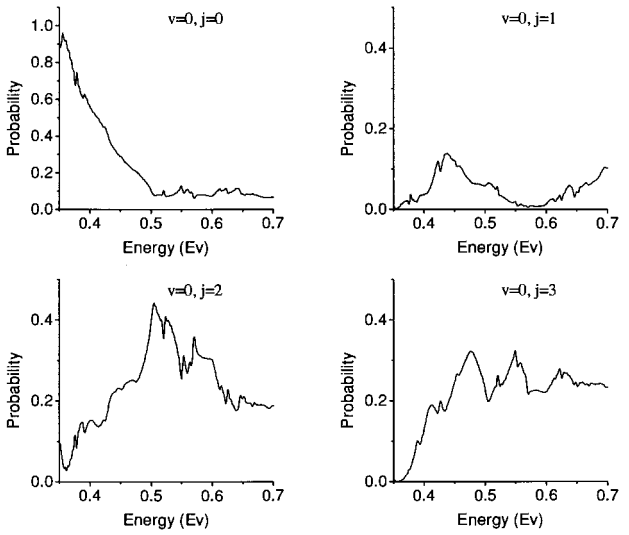

Figure 3. State-to-state inelastic probabilities $I[(\nu_0 = 0, j_0 = 0) \rightarrow (\nu, j)]$ for the Li + HF(ν_0, j_0) → LiF(ν, j) + H reaction, calculated by the TIW−RPD method.

TABLE 1: Grid, Wave Packet, and Expansion Parameters Used To Calculate the Results in Figures 2 and 3[a]

	grid dimensions				grid points			test functions		
	R_{min}	R_{max}	r_{min}	r_{max}	N_R	N_r	N_θ	R_0	R_l	k_{av}
s	4.0	18.0	0.7	3.5	164	6	30	13.5	0.25	16.0
q	1.2	8.0	0.7	8.0	79	81	30			
r	5.0	18.0	0.7	3.5	152	6	30	13.5	0.25	16.0
p	5.0	15.0	1.5	4.0	111	6	30	10.5	0.35	6.0

expansion paras			damping paras		initial wvpkt		
N	$\bar{H}$	ΔH	R_W	R_V	R_0	R_l	k_{av}
9000	0.75	0.75	1.0	3.0	13.5	0.25	−16.0

[a] All parameters are given in atomic units. The labels *p*, *q*, *r*, and *s* refer to the regions illustrated schematically in Figure 1. R_W is the width of the reflecting potential W_{qs}; R_V is the width of each of the absorbing potentials V_r, V_p, V_{rq}, and V_{pq}. All other parameters are either self-explanatory or are defined in the text.

given by

$$\chi_{\nu_0 l_0}(R, r, \theta|0) = \frac{1}{\sqrt{R_l \pi^{1/2}}} \exp\left(-\frac{(R - R_0)^2}{2R_l^2}\right) \exp(ik_{av}R)\phi_{\nu_0 l_0}(r)\hat{P}_{l_0}(\theta) \quad (10)$$

where $\phi_{\nu_0 l_0}(r)$ is a vibrational wave function of HF and $P_{l_0}(\theta)$ is a Legendre polynomial. Similar wave packets were employed as "test functions", with which to perform the final state analyses of $\xi_p^+(E)$ and $\xi_r^+(E) + \xi_s^+(E)$. Details of this procedure and of other aspects of the calculation not discussed here may be found in ref 1.

The absorbing potentials V_{rq}, V_{pq}, V_r, and V_p were all taken to be cubic ramps of the form given in ref 1. The reflecting potential, W_{qs}, took the form given in eq 9, with the ramp function $V_{ramp}(R)$ being taken as

$$V_{ramp}(R) = 0 \qquad R > R_{qs}$$
$$= 0.5 \qquad R \le R_{qs} \quad (11)$$

As discussed above, this choice of W_{qs} allows us to use the same basis set in the *s* region as in the *r* region.

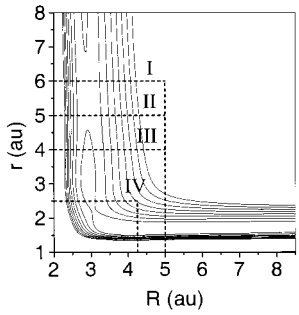

Figure 4. Cut through the Li + HF → LiF + H potential energy surface, plotted as a function of the reactant (Li + HF) Jacobi coordinates R and r, at $\theta = 74°$. Four different sizes of the *q* region are shown, which are enclosed by the dashed lines I−IV. The vertical lines pass through the reactant points-of-no-return, and the horizontal lines pass through the product points-of-no-return.

Convergence tests performed with respect to the numerical parameters given in Table 1 showed that the results of Figures 2 and 3 have converged to within better than a few percent. Note that, in the *p*, *r*, and *s* regions, only 6 quadrature points were required along the *r* coordinate, since, as expected, the DVRs obtained from the HF and LiF vibrational wave functions act as very efficient basis sets.

In Figure 5, we present a selection of results showing how the $[(\nu_0 = 0, j_0 = 0 \rightarrow (\nu = 0, j = 0)]$ reaction probabilities converge with respect to the reactant and product points-of-no-return. These calculations used the same grid spacings in R and r as the results of Figure 2, and a coarser grid spacing in θ (for which N_θ was set to 20). Similar convergence to that shown in Figure 5 was also found in the other (state-to-state) reaction probabilities and in the inelastic probabilities.

To be consistent with the recent calculation of Göğtas et al.,[11] we employed the Li + HF potential energy surface calculated by Parker et al.[12] and slightly modified by Göğtas et al.[11] We include the state-to-state reaction probabilities calculated by Göğtas et al. in Figure 2.

B. Results and Discussion. As we show in Figure 4, the potential energy surface for the Li + HF → LiF + H reaction has a long-range tail, with a well and a double barrier located along the product channel, and another well located along the reactant channel. These features are known[11,12] to support Feshbach resonances, which can extend down both the product and the reactant channel. When applying the TIW−RPD method to Li + HF, therefore, one could expect poor convergence with respect to the location of the points-of-no-return (PNRs), since, at a given resonance energy, the PNRs would have to be moved outward until the *q* (strong interaction) region enclosed the tail of the resonance wave function.

It is evident from Figure 5a,b, however, that the state-to-state reaction probabilities have converged very well with respect to the location of the product channel PNR. Similar convergence (not reported here) was obtained for the reactant channel PNR. As the PNR is moved outward from 4 to 5 au (Figure 5a), the fine structure of some of the resonances (for example, the peak located around 0.56 eV) changes only slightly. On moving from 5 to 6 au (Figure 5b), smaller changes occur at the same energies as when moving from 4 to 5 au. Figure 5c shows that even when the reactant and product PNRs are moved in to 4.25 and 2.5 au, the results are in good qualitative agreement with the results obtained with the reactant and product PNRs at 5 and 6 au.

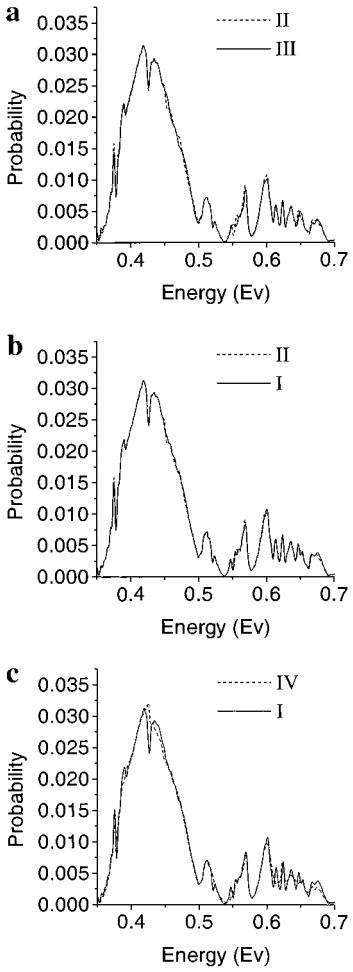

Figure 5. Convergence of the $R[(v_0 = 0, j_0 = 0) \rightarrow (v = 0, j = 0)]$ probabilities with respect to the size of the strong-interaction (q) region. Each plot compares the results of two TIW−RPD calculations that differed only with respect to the locations of the points-of-no-return. The points-of-no-return were located as indicated in Figure 4 by the labels (a) II and III, (b) I and II, and (c) I and IV.

For the Li + HF reaction, then, the application of the TIW−RPD method is very stable with respect to the location of the points-of-no-return. The calculation is evidently yielding good approximations to the resonance wave functions, even though, at some resonance energies, the wave function is undoubtedly being truncated by V_{rq} and V_{pq}. The effect of truncating the wave functions alters the fine structure of some of the resonance peaks but does not significantly alter the position, height, or shape of the peaks.

Given the good convergence with respect to the points-of-no-return (and with respect to the other parameters), it is somewhat surprising that the TIW−RPD results differ from the results of Gögtas et al.[11] by as much as 20% (see Figure 2). Regarding the position, shape, and relative heights of the peaks, the results are in excellent agreement, as may be seen by comparing, for example, the sharp dip in the $(00 \rightarrow 10)$ reaction probabilities at 0.52 eV. We suggest that the wave packet is being propagated correctly in both calculations but that a numerical error in the final state analysis part of one of the calculations is multiplying the results by a slowly varying function of energy. Probably the only significant difference between the two sets of results is in the fine structure of the resonance peaks. This difference is comparable to the difference in fine structure between the two curves in Figure 5a and is thus almost certainly a result of truncating the q region in the TIW−RPD calculation. Small differences between the two sets of results can also be expected to arise from the finite lengths of the absorbing potentials.

In addition to the work of Gögtas et al., accurate three-dimensional calculations on the Li + HF reaction have also been reported by Parker et al.[12] Our state-to-state reaction probabilities (and hence those of Gögtas et al.) differ qualitatively from those of Parker et al. at all energies above about 0.43 eV. We suggest that the results of Parker et al. were not converged above 0.43 eV. Parker et al. also reported state-to-state reaction probabilities in the 0.25−0.35 eV energy range, which consisted of a set of very narrow resonance peaks. We have not attempted to reproduce these results here, as the long lifetimes of the resonances would have required very long propagation times. At a later date, we intend to incorporate the TIW−RPD method into a filter diagonalization[20] method, which will enable us to calculate such very narrow resonances efficiently.

4. Conclusions

In this paper we have applied the TIW−RPD method to the Li + HF → LiF + H reaction. The resulting state-to-state reaction probabilities are found to be very stable with respect to the locations of the reactant and product points-of-no-return, even though the Li + HF potential energy surface is known to support long-lived Feshbach resonances that extend down the reactant and product channels. Accurately converged state-to-state reaction probabilities are obtained with the strong-interaction region enclosed in a box of dimensions 4 × 3 au. Good qualitative results are obtained with a box of dimensions 1.5 × 2.25 au. These dimensions should be contrasted with the asymptotic radii of the reaction, which were taken as 10.5 and 13.5 au.

The results clearly demonstrate that the TIW−RPD method is robust enough to be applied to reactions in which the dynamics are influenced by a long-range potential energy surface. At energies at which there is a resonance extending down the reactant and product channels, the partitioning of coordinate space (employed in the TIW−RPD method) approximates the resonance wave function by imposing outgoing boundary conditions on it at the points-of-no-return. Although this alters the fine structure of the resonance peaks (in the state-to-state reaction probabilities), it does not alter the height, shape, and position of the peaks. A similar effect, we assume, is also found when calculating cumulative reaction probabilities by the flux−flux autocorrelation (FFA) method of Seideman and Miller,[2] as the accuracy of both the FFA and the TIW−RPD method depends on how well the total flux out of the strong-interaction region has converged.

In future work we shall combine the TIW−RPD method with efficient basis sets and coordinate systems (probably based on hyperspherical coordinates[21,22]), and will develop efficient techniques for solving the strong-interaction part of the calculation. This will enable us to calculate state-to-state reaction probabilities for a variety of four- and five-atom reactions that are presently intractable by other methods.

Acknowledgment. We offer our congratulations and best wishes to Rafi Levine on the occasion of his 60th birthday. Kol hakavod uvrachot! We thank Drs. Antonio Laganà and Gabriel Balint-Kurti for discussing the Li + HF reaction with us and sending their potential energy subroutines. S.C.A. is supported under National Science Foundation Grant CHE-9700297. D.J.K. is supported in part under R.A. Welch Foundation Grant E-0608.

Partial support from the Petroleum Research Fund, administered by the American Chemical Society, is also acknowledged. The Ames Laboratory is operated for the Department of Energy by Iowa State University under Contract 2-7405-ENG82.

Appendix

The recursion relations used in the calculations of this paper differ from the ones given in ref 1 because, in this paper, we take W_{qs} to be a real, reflecting potential. The form of the recursion relations depends on the energy dependence of the $\Gamma(E)$ terms in eqs 4 and 5, which, in this paper, are taken to be

$$\Gamma_{\lambda q}(E) = -i\, V_{\lambda q}\, \Delta H \sin\phi \quad \text{with} \quad \lambda = r, p \tag{12}$$

It may then be shown (following refs 1 and 8) that the functions $\eta_{\lambda n}$, $\lambda = p, q, r, s$, of eq 7 satisfy the recursion relations

$$\eta_{sn} = 2(H_{\text{norm}} + \bar{W}_{qs})\eta_{sn-1} - \eta_{sn-2} \tag{13}$$

$$\eta_{qn} = \frac{1}{1 + V_{\text{tot}}}[2H_{\text{norm}}\eta_{qn-1} - (1 - V_{\text{tot}})\eta_{qn-2} - 2\bar{W}_{qs}\eta_{sn-1}] \tag{14}$$

$$\eta_{\lambda n} = 2H_{\text{norm}}\eta_{\lambda n-1} - \eta_{\lambda n-2} + V_{\lambda q}(\eta_{qn} - \eta_{qn-2}) \qquad \lambda = p, r \tag{15}$$

where $V_{\text{tot}} = V_{rq} + \sum_p V_{pq}$ and $\bar{W}_{qs} = W_{qs}/\Delta H$.

References and Notes

(1) Althorpe, S. C.; Kouri, D. J.; Hoffman, D. K. *J. Chem. Phys.* **1997**, *107*, 7816.

(2) Seideman, T.; Miller, W. H. *J. Chem. Phys.* **1992**, *97*, 2499; for a wave packet version of this method see, Zhang, D. H.; Light, J. C. *J. Chem. Phys.* **1996**, *104*, 6184.

(3) Neuhauser, D.; Baer, M. *J. Chem. Phys.* **1989**, *90*, 4351; Neuhauser, D.; Baer, M.; Judson, R. S.; Kouri, D. J. **1989**, *90*, 5882; *Comput. Phys. Commun*. **1990**, *63*, 460.

(4) Peng, T.; Zhang, J. Z. H. *J. Chem. Phys.* **1996**, *105*, 6072; Zhu, W.; Peng, T.; Zhang, J. Z. H. *J. Chem. Phys.* **1997**, *106*, 1742.

(5) Kouri, D. J.; Hoffman, D. K.; Peng, T.; Zhang, J. H. Z. *Chem. Phys. Lett.* **1996**, *262*, 519.

(6) For a general introduction to the TIW approach to quantum scattering see Kouri, D. J.; Hoffman, D. K. Few-Body Systems **1995**, *18*, 203, and Kouri, D. J.; Huang, Y.; Hoffman, D. K. In *Dynamics of Molecules and Chemical Reactions*; Wyatt, R. E., Zhang, J. Z. H., Eds.; Marcel Dekker Inc.: New York, 1996.

(7) Althorpe, S. C. Kouri, D. J.; Hoffman, D. K.; Zhang, J. Z. H. *J. Chem. Soc., Faraday Trans.* **1997**, *93*, 703.

(8) Althorpe, S. C.; Kouri, D. J.; Hoffman, D. K. *J. Chem. Phys.* **1997**, *106*, 7629.

(9) Althorpe, S. C.; Kouri, D. J.; Hoffman, D. K. *Chem. Phys. Lett.* **1997**, *275*, 173.

(10) Tal-Ezer, H.; Kosloff, R. *J. Chem. Phys.* **1984**, *81*, 3967.

(11) Gögtas, F.; Balint-Kurti, G. G.; Offer, A. R. *J. Chem. Phys.* **1996**, *104*, 7927.

(12) Parker, G. A.; Pack, R.; Laganà, A. *Chem. Phys. Lett.* **1993**, *202*, 75; Parker, G. A.; Laganà, A.; Crocchianti, S.; Pack, R. T. *J. Chem. Phys.* **1995**, *102*, 1238.

(13) As we showed in ref 1, W_{qs} may be taken as an absorbing potential or a reflecting potential, or both. The only constraint on W_{qs} is that it must prevent the wave packet from reaching the boundaries of the *s* region.

(14) Note that eqs 2−5 differ slightly from the TIW−RPD equations given in ref 1 because W_{qs} is taken to be real in this paper.

(15) The energy-dependent factors in the $\Gamma(E)$ potentials govern the form taken by the Chebyshev-like recursion relations—see ref 1 for details.

(16) Hoffman, D. K.; Marchioro II, T. L.; Arnold, M.; Huang, Y.; Zhu, W.; Kouri, D. J. *J. Math. Chem.* **1996**, *20*, 117, and references therein.

(17) Wei, G. W.; Althorpe, S. C.; Zhang, D. S.; Kouri, D. J.; Hoffman, D. K. *Phys. Rev. A* **1998**, *57*, 3309.

(18) Wei, G. W.; Althorpe, S. C.; Kouri, D. J.; Hoffman, D. K. *J. Chem. Phys.* **1998**, *108*, 7065.

(19) Bacic, Z.; Light, J. C. *Annu. Rev. Phys. Chem.* **1989**, *40*, 469.

(20) Neuhauser, D. *J. Chem. Phys.* **1994**, *100*, 5076; Kroes, G.-J.; Wall, M. R.; Pang, J. W.; Neuhauser, D. *J. Chem. Phys.* **1997**, *106*, 1800.

(21) Pack, R.; Parker, G. A. *J. Chem. Phys.* **1987**, *87*, 3888.

(22) Pogrebnya, S. K.; Echave, J.; Clary, D. C. *J. Chem. Phys.* **1997**, *107*, 8975.